Original Articles

Texture Analysis of Fluorescence Lifetime Images of Nuclear DNA with Effect of Fluorescence Resonance Energy Transfer

Shin-ichi Murata, Petr Herman, and Joseph R. Lakowicz*

Center for Fluorescence Spectroscopy, Department of Biochemistry and Molecular Biology, University of Maryland at Baltimore, School of Medicine, Baltimore, Maryland

Received 5 July 2000; Revision Received 2 October 2000; Accepted 14 October 2000

Background: Fluorescence lifetime imaging microscopy (FLIM) is becoming an important tool in cellular imaging. In FLIM, the image contrast is concentration insensitive, whereas it is sensitive to the local environment and interactions of fluorophores such as fluorescence resonance energy transfer (RET).

Methods: Fluorescence microscopy, lifetime imaging, and texture analysis were used to study the spatial distribution of fluorophores bound to nuclear DNA. 3T3-Swiss albino mice fibroblast nuclei were labeled with Hoechst 33258 (Ho), an AT-specific dye, and 7-aminoactinomycin D (7-AAD), a GC-specific dye. Ho is a RET donor to the 7-AAD acceptor.

Results: Texture analysis of 50 alcohol-fixed nuclei quantitatively showed changes of spatial distribution of apparent donor lifetimes. RET increased the spatial heterogeneity in the phase and modulation lifetime images. In most of the doubly stained cells (about 80%), the phase and modulation lifetime distributions were spatially homogeneous. In about 20% of the cells, we noticed that lower phase and modulation lifetimes caused by RET were correlated with regions of high Ho intensity in the nuclei.

Conclusions: The spatial lifetime heterogeneity of Ho in presence of 7-AAD seems to be caused by RET between closely spaced strands in the three dimensionally condensed regions of DNA. Cytometry 43:94–100, 2001.

Key terms: 3T3 fibroblasts; Hoechst 33258; 7-aminoactinomycin D; cell cycle

Fluorescence staining of DNA is widely used in spectroscopy (1–4) and in microscopy (5,6). Fluorescent dyes bound to DNA are also widely used in DNA sequencing (7,8), for genetic analysis by fluorescence in situ hybridization (9–12), and in analysis of DNA structure using resonance energy transfer (RET; 13–16). Time-resolved studies of probes bound to DNA have shown that the probe lifetimes often increase upon binding to DNA (17,18) and that the decay times are sensitive to RET (19,20).

During the past 10 years, a new method of cellular imaging has become available, fluorescence lifetime imaging microscopy (FLIM; 21–26). In FLIM, the image contrast is independent of the local intensity of the stained cell; instead, it is based on the fluorescence lifetime in each region of the cell. Lifetime-based contrast is valuable because the lifetimes of probes often depend on their local environment or the presence of a specific analyte. For instance, the lifetimes of the calcium-specific probes Quin-2 and Calcium Green are known to increase upon binding to calcium. For cells labeled with Quin-2 or Calcium Green, the lifetime images reveal the spatial distribution of calcium and are mostly independent of the local probe concentrations (24,25).

In this study, we extend the concept of FLIM to imaging of cell nuclei from 3T3 fibroblasts. The nuclei were labeled with either Hoechst 33258 (Ho) or with both Ho

Grant sponsor: National Center for Research Resources; Grant number: RR-08119; Grant sponsor: National Institutes of General Medical Science; Grant number: GM-35154.

Shin-ichi Murata is on leave from the First Department of Pathology, Kyoto Prefectural University of Medicine, 456 Kajii-cyo Hirokoji Kawaramachi Kamikyo-ku, Kyoto, 602, Japan.

Petr Herman is on leave from the Institute of Physics, Charles University, Ke Karlovu 5, 121 16 Prague 2, Czech Republic.

*Correspondence to: Joseph R. Lakowicz, Center for Fluorescence Spectroscopy, Department of Biochemistry and Molecular Biology, University of Maryland at Baltimore, School of Medicine, 725 West Lombard Street, Baltimore, MD 21201.

E-mail: jf@cfs.umbi.umd.edu

and 7-aminoactinomycin D (7-AAD). Ho binds specifically to AT-rich regions of DNA and 7-AAD binds preferentially to GC-rich regions of DNA (27,28). Ho is a RET donor to 7-AAD. The chosen pair of Ho and 7-AAD shows a good spectral match required by RET (29). The Förster distance of this donor-acceptor pair is 40 Å (28). We measured intensity and lifetime images of Ho in the absence and presence of the 7-AAD acceptor. These images were subjected to texture analysis (30,31) to evaluate the effect of RET from Ho to 7-AAD on the angular second moment, sum variance, and difference variance in the intensity and lifetime images. The effects of RET on these parameters of texture analysis were then interpreted in terms of spatial proximity of Ho and 7-AAD in the nuclear DNA.

MATERIALS AND METHODS

Cells and Culture Conditions

Mouse fibroblasts (3T3-Swiss albino) were grown at 37°C in the bottom-glass dishes (Mat Tek, Ashland, MA) containing Dulbecco's modified Eagles's medium with 10% calf serum.

Fixation and Cell Staining

The cells in the dishes were fixed in 70% ethanol (4°C, at least 30 min). After rinsing, the cells were stained by 0.4 μM Ho and 0.8 μM 7-AAD, which were used as donor and acceptor, respectively. Ho and 7-AAD were obtained from Molecular Probes (Eugene, OR). All the experiments were carried out at room temperature in 10 mM Tris-HCl buffer, pH 7.5, containing 100 mM NaCl.

Measurement Condition of Fluorescence Intensity and Lifetime Imaging

The principles of operation of the homodyne FLIM technique were described previously (21). The apparatus was built around the Axiovert 135TV inverted fluorescence microscope (Carl Zeiss, Thornwood, NY). The picosecond light pulses at 335 nm from the frequency-doubled synchronously pumped DCM dye laser were directed to the microscope using a quartz optical fiber. The epi-illumination was accomplished by the Zeiss C-Apochromat water immersion objective, 40×/1.2 w, with a 1.6× Optovar insert and the Zeiss FT 395 dichroic beam splitter. Fluorescence from the sample was isolated by the 450DF65 interference filter (Omega Optical, Brattleboro, VT) and quantitized using a C5825 high-speed modulated image intensifier (Hamamatsu, Bridgewater, NJ) and a PXL scientific-grade, slow-scan, cooled CCD camera (Photometrics, Tucson, AR). The gain of the intensifier was modulated at 113.202 MHz using an output of the PTS 300 synthesizer (Programmed Test Sources, Littleton, MA). The synthesizer was phase locked to the master-oscillator of the pumping Ar^+ laser mode-locker. For each lifetime measurement, eight images with the detector phase equally spaced over 360° were acquired and analyzed by a method described elsewhere (25). The illumination level of the sample was decreased by a neutral-density filter to the level that the acquisition time for the images was in the order of seconds. No detectable photobleaching was observed under these conditions.

Measurement of Fluorescence Intensity and Lifetime Imaging

The positions of 50 cells on a bottom-glass dish were recorded and assigned numbers. The cells were stained by 0.4 μM Ho and their fluorescence intensity and lifetime imaging were measured. Then 0.8 μM 7-AAD was added to the same dish for fluorescence RET measurement. The fluorescence intensity and lifetime images of the same 50 cells double stained with Ho and 7-AAD were measured individually.

Texture Analysis Using Co-Occurrence Matrix

The program for texture analysis was written in C language. The program calculated 14 texture parameters from the co-occurrence matrices (30), which were constructed from gray-level images after reduction from 16 to 8-bit gray levels and normalization to the same average values. The following three parameters were selected as independent descriptors of the Ho staining pattern. The angular second moment (Eq. 1) shows spatial homogeneity, the sum variance (Eq. 2) reveals spatial heterogeneity, and difference variance (Eq. 3) describes the contrast of the Ho staining pattern. These values were calculated using:

$$ASM = \sum_{i=1}^{Ng} \sum_{j=1}^{Ng} \{P(i,j)\}^2 \quad (1)$$

$$S\ Var = \sum_{k=2}^{2\,Ng} \left(k - \sum_{k=2}^{2\,Ng} k \cdot P_{x+y}(k) \right)^2 \cdot P_{x+y}(k) \quad (2)$$

$$D\ Var = \sum_{k=0}^{Ng} \left(k - \sum_{k=0}^{Ng} k \cdot P_{x-y}(k) \right)^2 \cdot P_{x-y}(k) \quad (3)$$

where $P_{x+y}(k)$ and $P_{x-y}(k)$ are defined as follows (30).

$$P_{x+y}(k) = \sum_{\substack{i=1 \\ i+j=k}}^{Ng} \sum_{j=1}^{Ng} P(i,j) \quad k = 2, 3 \ldots, 2\,Ng \quad (4)$$

$$P_{x-y}(k) = \sum_{\substack{i=1 \\ |i-j|=k}}^{Ng} \sum_{j=1}^{Ng} P(i,j) \quad k = 0, 1, \ldots, Ng-1 \quad (5)$$

The term P(i, j) is the (i,j)th entry in a normalized gray-tone spatial-dependence matrix (co-occurrence matrix) and Ng is the number of distinct gray levels in the quantized image. These three parameters (ASM, SVar, and DVar) are calculated from every nuclear image of the 50

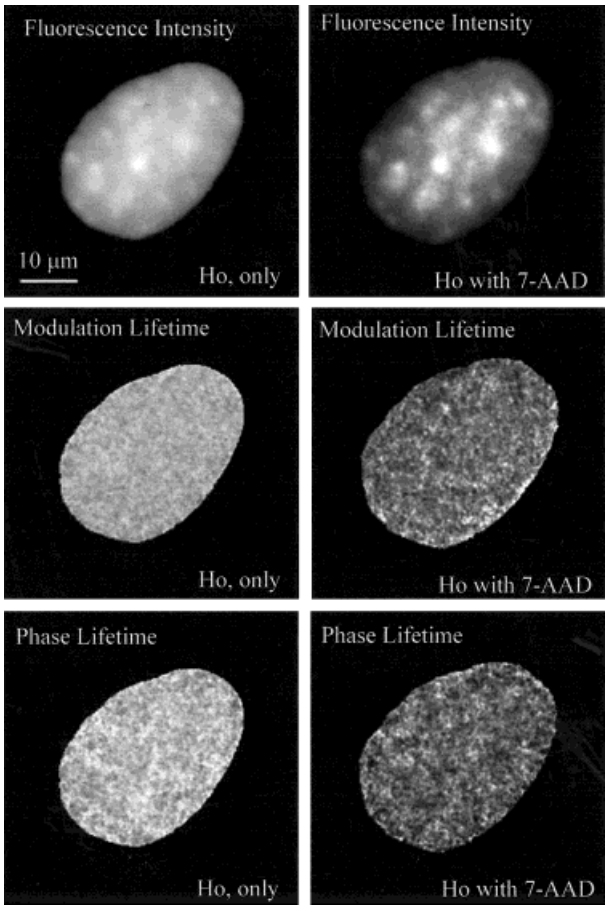

FIG. 1. Nuclear images of fluorescence intensity and lifetime in cell stained with Ho in the presence or absence of 7-AAD. After the addition of 7-AAD, the lifetime images became slightly more heterogeneous and the cell showed weak correlation between fluorescence intensity and lifetime.

cells, which were stained by Ho in the absence and presence of 7-AAD.

RESULTS

The nuclei stained with Ho, the AT-specific dye, were strongly fluorescent and the images were detectable without significant nonspecific background fluorescence from the cytoplasm. Intensity images of Ho-stained nuclei are shown in Figures 1 and 2. The nuclei displayed regions of higher and lower intensity. Given the base specificity of Ho, the higher intensity regions probably correspond to regions of higher AT base pair concentrations in the nuclei. In contrast to the intensity images, the phase and modulation images were flat and within resolution of our microscopy images did not display significant spatial variations. This result is consistent with the known behavior of Ho, which prefers AT-base pairs and then displays the same lifetimes whenever bound to DNA.

Addition of the acceptor 7-AAD to the nuclei resulted in a decrease in the intensity and lifetime of the DNA-bound Ho (29; Figures 3–5). Following the addition of 7-AAD, 80–90% of the cells displayed a flat lifetime image by both phase and modulation (Fig. 1). This result indicates that, on average, the 7-AAD molecules are found and distanced comparable to the Förster distance R_0 from Ho. In interphase cells, which were used in this study, the chromosomes with AT- and GC-rich regions are three dimensionally intermingled (32). For this three-dimensional distribution of chromosomes and our acceptor concentration, the 7-AAD molecules are found and distanced comparable to the Förster distance R_0 from Ho as described in Murata et al. (29). Additionally, a flat lifetime image suggests that there is no significant spatial difference in the AT to GC base content in the nuclei to within the resolution of the microscopy images.

The remaining 10–20% of the nuclei displayed spatially heterogeneous phase and modulation lifetimes (Fig. 2). More specifically, the phase and modulation lifetimes are lower in regions of higher Ho intensity. Apparently in this subpopulation of cells, the extent of RET from Ho to 7-AAD is higher in regions of locally higher AT concentrations.

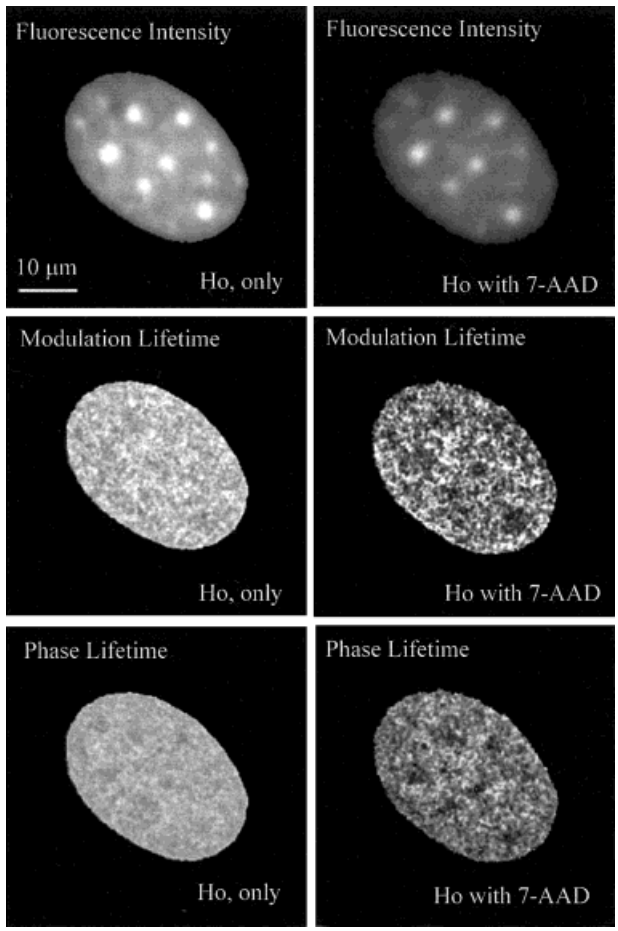

FIG. 2. Fluorescence intensity and lifetime images of another cell stained with Ho in the presence and absence of 7-AAD. After the addition of 7-AAD, the lifetime image becomes strongly heterogeneous. This cell shows more obvious correlation between fluorescence intensity and lifetime than the cell in Figure 1.

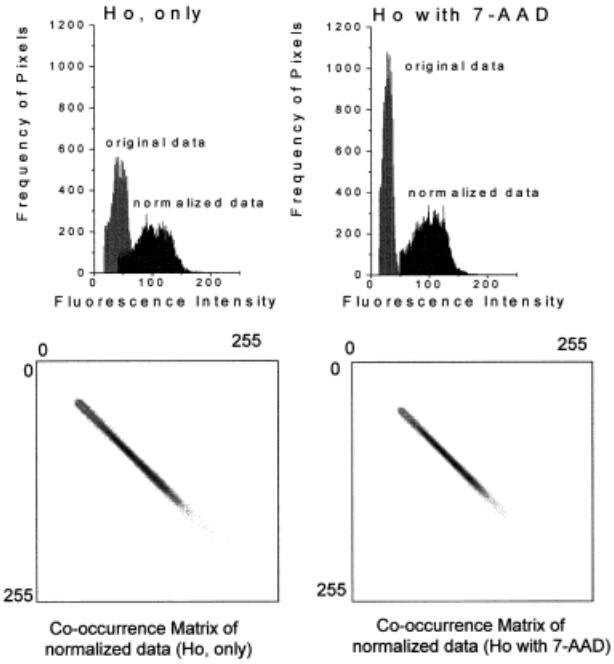

FIG. 3. Histograms and co-occurrence matrices of fluorescence intensity images from the cell shown in Figure 1. The cell was stained with Ho in the presence and absence of 7-AAD. Co-occurrence matrices were constructed from images normalized to the same average fluorescence intensity.

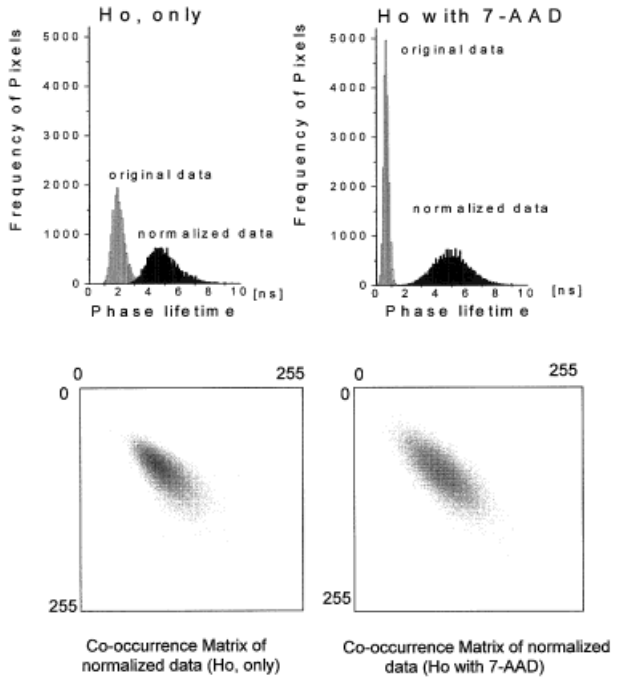

FIG. 5. Histograms and co-occurrence matrices of phase lifetime images from the cell shown in Figure 1. Cell was stained with Ho in the presence and absence of 7-AAD. Co-occurrence matrices were constructed from images normalized to the same average phase lifetime.

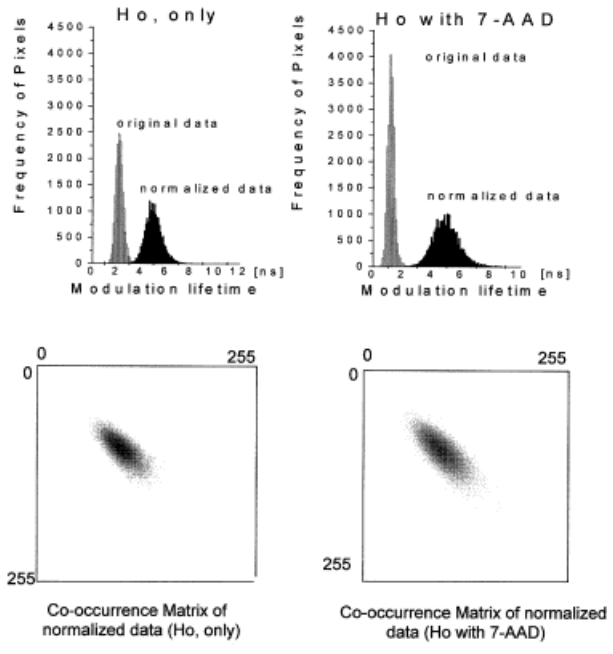

FIG. 4. Histograms and co-occurrence matrices of modulation lifetime images from the cell shown in Figure 1. The cell was stained with Ho in the presence and absence of 7-AAD. Co-occurrence matrices were constructed from the images normalized to the same average modulation lifetime.

To obtain a quantitation measurement of spatial heterogeneity in the nuclei, we used texture analysis (30,31). For this purpose, the intensity phase and modulation images were normalized (Figs. 3–5). The intensity histograms show that 7-AAD decreased the Ho intensity, which is a good indication for the occurrence of RET. Visual examination of the normalized intensity histogram shows no discernible difference in the absence or presence of 7-AAD (Fig. 3). The presence of 7-AAD results in a modest decrease in the range of intensities, as seen from the decrease in length of the ASM scattergram from NW to SE (Fig. 3). There also appears to be a minor decrease in contrast, as seen from a slightly decreased width in the perpendicular direction.

Different results were observed for the effects of 7-AAD on the phase and modulation lifetimes (Figs. 4, 5). The unnormalized histograms show a decrease in the phase and modulation lifetimes due to 7-AAD (Figs. 4, 5). The normalized histograms are more informational and show an increased width of the lifetime distributions in the presence of 7-AAD (Figs. 4, 5). The ASM scattergrams are somewhat elongated (NW to SE) in the presence of 7-AAD, which also reflects a wide distribution of lifetimes. Examination of the perpendicular width suggests a minor increase in contrast for this single nucleus.

In order to test our visual impressions, we averaged the results of the texture analysis for all 50 nuclei for the intensity (Fig. 6), modulation lifetime (Fig. 7), and phase lifetimes (Fig. 8). For the intensity images (Fig. 6), the

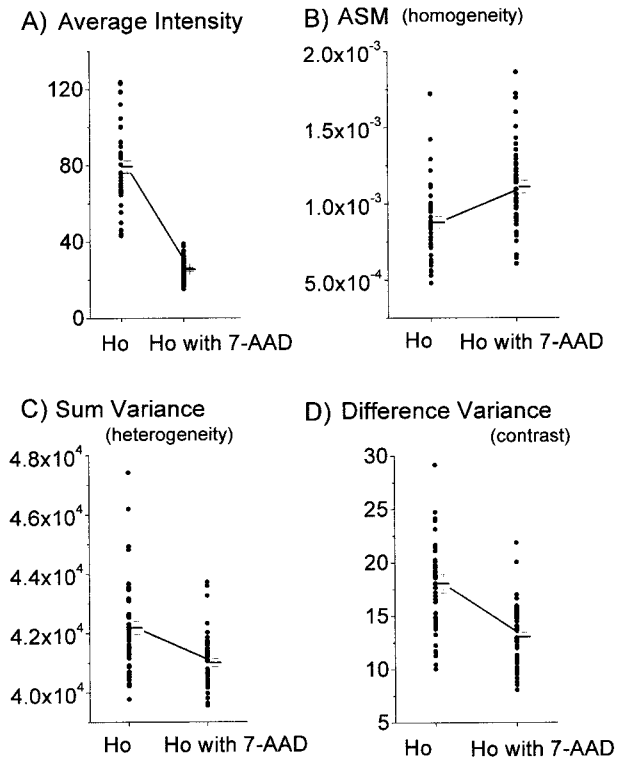

FIG. 6. Scattergrams of the texture analysis results collected from the fluorescence intensity images of 50 different cells. Closed circles represent results from individual cells. Error bars indicate mean value with SE. **A:** Original fluorescence intensity data. **B–D:** Texture analysis results of normalized images.

presence of 7-AAD decreased the intensity (Fig. 6A), increased the homogeneity (Figs. 6B,C), and decreased the contrast (Fig. 6D). Distinct results were found for the modulation and phase images (Figs. 7, 8). The presence of 7-AAD decreased the lifetime (Figs. 7A, 8A), but increased the spatial heterogeneity (Figs. 7B,C, 8B,C), and contrast (Figs. 7D, 8D). Taken together, the effects of RET on the three parameters (ASM, Svar, and DVar) suggest that RET quenching of Ho is not spatially heterogeneous and that regions of higher DNA density, both AT and GC pairs, are present in select regions of the nuclei.

Figure 9 shows correlation between RET efficiency and contrast (the difference variance) of the modulation lifetime image. The contrast of the lifetime image seems to increase with decreasing mean efficiency of RET. Because the cells with lower RET efficiency are expected to have less condense DNA and larger average donor-to-acceptor distance, some donors seem to be partiallly quenched.

We have also found that RET efficiency depends on the cell cycle. Cells in G_2/M phase show slightly higher RET efficiency than the cells in $G_{0/1}$ phase (Fig. 10). At this moment, we do not know whether the increased energy transfer is due to a higher density of the DNA condensation centers or to spatial redistribution of the AT- and GC-rich regions of DNA. Such cell cycle-dependent redistribution could change base pair composition of the centers in favor of GC base pairs and increase RET efficiency.

DISCUSSION

We interpreted the changes in intensity and lifetime images after addition of 7-AAD in terms of the local AT- and GC-rich DNA concentration. On the other hand, we must also consider lifetime heterogeneity of donor decay. It is well known that RET between donors and acceptors bound to DNA results in increased lifetime heterogeneity in the phase and modulation values, depending on acceptor concentration (19,20). This effect would result in a range of decay times due to the nonexponential donor decays. However, irrespective of the lifetime heterogeneity of the donor decays, the phase and modulation values, measured at a single light modulation frequency, results in a unique apparent phase and modulation lifetime (33). For a multiexponential or nonexponential decay, the apparent phase lifetime is always shorter than the apparent modulation lifetime (29,34,35), as seen for Ho in Figures 7 and 8. Unfortunately, we cannot recover the true values of nonexponential fluorescence decay using FLIM at a single light modulation frequency. However, our goal was to search for variations of the distance between the Ho donor and the 7-AAD acceptor in individual nuclei. We can study such changes by quantification of spatial variations of apparent donor lifetimes in the presence and absence of the acceptor, which were shown to be directly related to the nonexponential lifetime decay and RET efficiency.

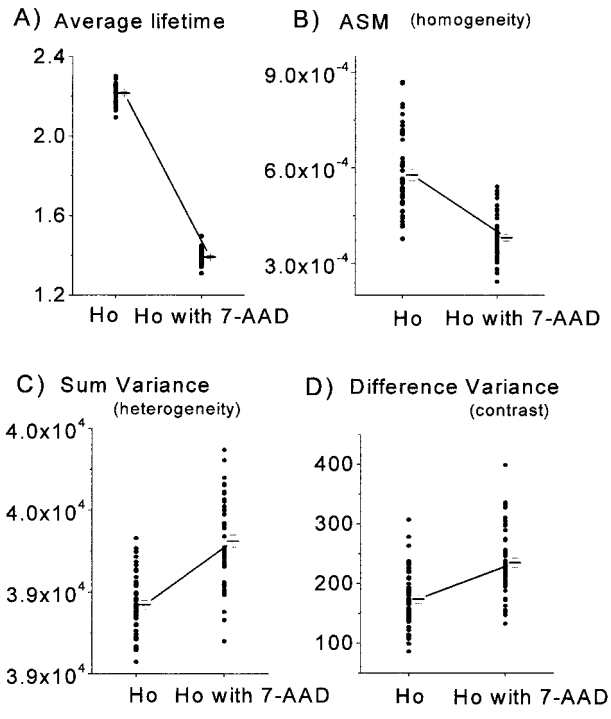

FIG. 7. Scattergrams of the texture analysis results collected from the modulation lifetime images of 50 cells. Closed circles represent the results from individual cells. The error bars indicate mean values with SE. **A:** Original lifetime data. **B–D:** Texture analysis results of normalized images. The presence of 7-AAD reduced the average Ho modulation lifetimes from 2.3 to 1.4 ns.

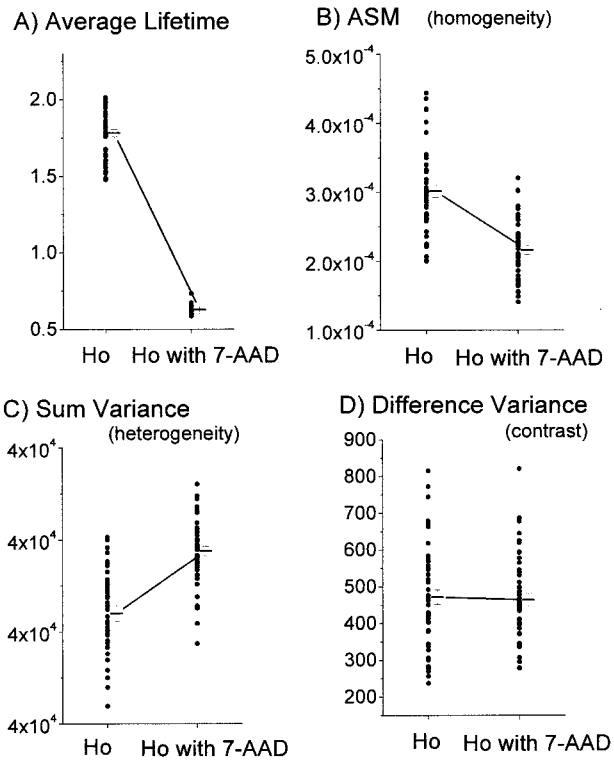

FIG. 8. Scattergrams of the texture analysis results collected from the phase lifetime images of 50 cells. Closed circles represent results from individual cells. Error bars indicate mean values with SE. **A:** Original lifetime data. **B–D:** Texture analysis results of normalized images. The presence of 7-AAD reduced the average phase lifetime from1.8 to 0.6 ns.

In conclusion, the results of the texture analysis revealed higher heterogeneity of the lifetime images in the presence than in the absence of 7-AAD. In about 20% of the cells, we could visually find a spatial lifetime variation that is represented by lower regions in the nuclear lifetime

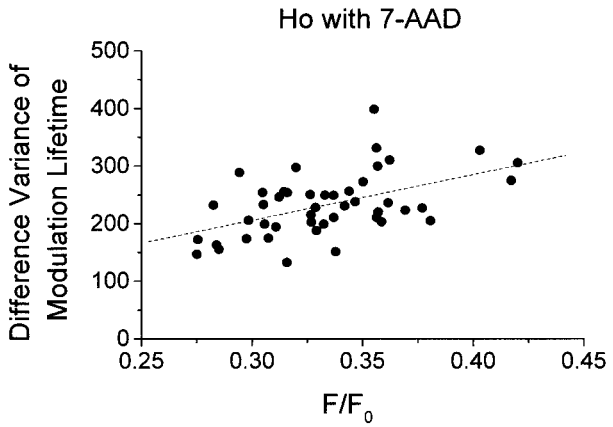

FIG. 9. Relation between the efficiency of the energy transfer and the difference variance of the modulation lifetime. The data points represent 50 nuclei double stained by Ho and 7-AAD. F_0 represents the average fluorescence intensity with Ho only; F represents the average fluorescence intensity with Ho and 7-AAD

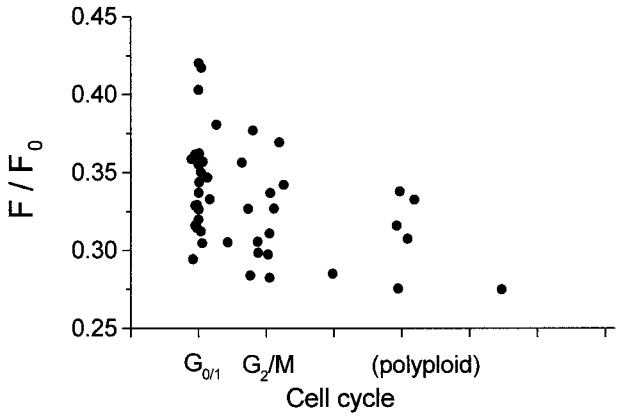

FIG. 10. Relation between cell cycle and energy transfer efficiency. F_0 is an average fluorescence intensity of cells stained with Ho only; F is an average fluorescence intensity of cells stained with Ho and 7-AAD.

images in the presence of the acceptor (Fig. 2). In these regions, which correspond to the AT-rich DNA regions as seen from the intensity images (Fig. 2), the RET efficiency is higher because lifetime images of donor-only stained nuclei are flat. Such a result indicates that the average distance between Ho and 7-AAD is small in these regions of the nuclei. It is well known that the AT-rich regions of DNA are more condensed than the GC-rich regions (32). It seems probable that the spatial lifetime heterogeneity of Ho in the presence of 7-AAD is due to the closely spaced DNA strands in these three dimensionally condensed regions, rather than due to the RET between more closely spaced donors and acceptors in the same DNA helix.

LITERATURE CITED

1. Ellerton NF, Isenberg I. Fluorescence polarization study of DNA-proflavine complexes. Biopolymers 1969;8:767–786.
2. Steiner RF, Kubota Y. Fluorescent dye-nucleic acid complexes. In: Steiner RF, editor. Excited states of biopolymers. New York: Plenum Press; 1983. p 203–254.
3. Suh D, Chaires JB. Criteria for the mode of binding of DNA binding agents. Bioorg Med Chem 1995;3:723–728.
4. LePecq J-B, Paoletti C. A fluorescent complex between ethidium bromide and nucleic acids. Physical-chemical characterization. J Mol Biol 1967;27:87–106.
5. Latt-SA. Detection of DNA synthesis in interphase nuclei by fluorescence microscopy. J Cell Biol 1974;62:546–550.
6. Urata Y, Itoi H, Murata S, Konishi E, Ueda K, Azumi Y, Ashihara T. From cytofluorometry to fluorescence image analysis. Acta Histochem Cytochem 1991;24:367–374.
7. Smith LM, Sanders JZ, Kaiser RJ, Hughes P, Dodd C, Connell CR, Heiner C, Kent SBH, Hood LE. Fluorescence detection in automated DNA sequence analysis. Nature 1986;321:674–679.
8. Prober JM, Trainor GL, Dam RJ, Hobbs FW, Robertson CW, Zagursky RJ, Cocuzza AJ, Jensen MA, Baumeister K. A system for rapid DNA sequencing with fluorescent chain-terminating dideoxynucleotides. Science 1987;238:336–343.
9. Tkachuk DC, Pinkel D, Kuo W-L, Weier H, Gray JW. Clinical applications of fluorescence in situ hybridization GATA 1991;8:67–74.
10. Denijn M, Schuurman H-J, Jacobse KC, De Weger RA. In situ hybridization: a valuable tool in diagnostic pathology. APMIS 1992;100:669–681.
11. Popescu NC, Zimonjic DB. Molecular cytogenetic characterization of cancer cell alterations. Cancer Genet Cytogenet 1997;93:10–21.
12. Swiger RR, Taylor JD. Fluorescence in situ hybridization. Environ Mol Mutagen 1996;27:245–254.
13. Jares-Erijman EA, Jovin TM. Determination of DNA helical handedness

by fluorescence resonance energy transfer. J Mol Biol 1996;257:597–617.
14. Mergny J-L, Garestier T, Rougee M, Lebedev AV, Chassignol M, Thuong NT, Helene C. Fluorescence energy transfer between two triple helix-forming oligonucleotides bound to duplex DNA. Biochemistry 1994; 33:15321–15329.
15. Gohlke C, Murchie AIH, Lilley DMJ, Clegg RM. Kinking of DNA and RNA helices by bulged nucleotides observed by fluorescence resonance energy transfer. Proc Natl Acad Sci USA 1994;91:11660–11664.
16. Rye HS, Yue S, Wemmer DE, Quesada MA, Haugland RP, Mathies RA, Glazer AN. Stable fluorescent complexes of double-stranded DNA with bis-intercalating asymmetric cyanine dyes: properties and applications. Nucleic Acids Res 1992;20:2803–2812.
17. Ashikawa I, Kinosita K, Ikegami A. Increased stability of the higher order structure of chicken erythrocyte chromatin: nanosecond anisotropy studies of intercalated ethidium. Biochemistry 1985; 24: 1291–1297.
18. Malatesta V, Andreoni A. Dynamics of anthracyclines/DNA interaction: a laser time-resolved fluorescence study. Photochem Photobiol 1988;48:409–415.
19. Murata S, Kusba J, Piszczek G, Gryczynski I, Lakowicz JR. Donor fluorescence decay analysis for energy transfer in double-helical DNA with various acceptor concentrations. Biospectroscopy (in press).
20. Maliwal BP, Kusba J, Lakowicz JR. Fluorescence energy transfer in one dimension: frequency domain fluorescence study of DNA. Biopolymers 1995;35:245–255.
21. Lakowicz JR, Berndt KW. Lifetime-selective fluorescence imaging using an rf phase-sensitive camera. Rev Sci Instrum 1991;62:1727–1734. (Reprinted in SPIE Milestone Series on Optical Tomography 1997)
22. Gerritsen H, Draaijer A. Second International Lifetime Imaging Meeting, Utrecht, Netherlands, June 14, 1996. J Fluoresc 1997;7:1–99.
23. Lakowicz JR, Szmacinski H, Nowazcyk K, Berndt K, Johnson ML. Fluorescence lifetime imaging. Anal Biochem 1992;202:316–330.
24. Lakowicz JR, Szmacinski H, Johnson ML. Calcium concentration imaging using fluorescence lifetimes and long-wavelength probes. J Fluoresc 1992;2:47–62.
25. Lakowicz JR, Szmacinski H, Nowaczyk K, Lederer WJ, Kirby MS, Johnson ML. Fluorescence lifetime imaging of intracellular calcium in COS cells using QUIN-2. Cell Calcium 1994;15:7–27.
26. Straub M, Hell SW. Fluorescence lifetime three-dimensional microscopy with picosecond precision using a multifocal multiphoton microscope. Appl Phys Lett 1998;73:1769–1771.
27. Sailer BL, Nastasi AJ, Valdez JG, Steinkamp JA, Crissman HA. Differential effects of deuterium oxide on the fluorescence lifetimes and intensities of dyes with different modes of binding to DNA. Histochem Cytochem 1997;45:165–175.
28. Elhanan S, Saumel AL. Energy transfer and binding composition between dyes used to enhance staining differentiation in metaphase chromosomes. Chromosoma 1980;79:1–28.
29. Murata S, Herman P, Lin H-J, Lakowicz JR. Fluorescence lifetime imaging of nuclear DNA: effect of fluorescence resonance energy transfer. Cytometry (in press).
30. Haralick RM, Shanmugam K, Dinstein I. Textural features for image classification. IEEE Trans Systems Man Cybernet 1973;SMC3(6):610–621.
31. Santisteban MS, Brugal G. Fluorescence image analysis of the MCF-7 cycle related changes in chromatin texture. Anal Cell Pathol 1995;9: 13–28.
32. Alberts B, Bray D, Lewis J, Raff M, Roberts K, Watson JD. Molecular biology of the cell, 3rd edition. New York: Garland Publishing; 1994. p 335–354.
33. Lakowicz JR. Principles of fluorescence spectroscopy, 2nd edition. New York: Kluwer Academic/Plenum; 1999. 698 p.
34. Kilin SF. The duration of photo- and radioluminscence of organic compounds. Optical Spectroscopy 1962;12:414–416.
35. Spencer RD, Weber G. Measurement of subnanosecond fluorescence lifetimes with a cross-correlation phase fluorometer. Ann N Y Acad Sci 1969;158:361–376.